Towards Standardized Acquisition with a Dual-probe Ultrasound Robot for Fetal Imaging

James Housden[1], Shuangyi Wang[2], Xianqiang Bao[1], Jia Zheng[3], Emily Skelton[1], Jacqueline Matthew[1], Yohan Noh[4], Olla Eltiraifi[1], Anisha Singh[5], Davinder Singh[5], and Kawal Rhode[1]

***Abstract*—Standardized acquisitions and diagnoses using robots and AI would potentially increase the general usability and reliability of medical ultrasound. Working towards this prospect, this paper presents the recent developments of a standardized acquisition workflow using a novel dual-probe ultrasound robot, for a project known as intelligent Fetal Imaging and Diagnosis (iFIND). The workflow includes an abdominal surface mapping step to obtain a non-parametric spline surface, a rule-based end-point calculation method to position each individual joint, and a motor synchronization method to achieve a smooth motion towards a target point. The design and implementation of the robot are first presented in this paper and the proposed workflow is then explained in detail with simulation and volunteer experiments performed and analyzed. The closed-form analytical solution to the specific motion planning problem has demonstrated a reliable performance controlling the robot to move towards the expected scanning areas and the calculated proximity of the robot to the surface shows that the robot maintains a safe distance while moving around the abdomen. The volunteer study has successfully demonstrated the reliable working and controllability of the robot in terms of acquiring desired ultrasound views. Our future work will focus on improving the motion planning, and on integrating the proposed standardized acquisition workflow with newly-developed ultrasound image processing methods to obtain diagnostic results in an accurate and consistent way.**

***Index Terms*—Medical robots and systems, motion and path planning, software-hardware integration for robot systems**

I. Introduction

Medical ultrasound is an important imaging modality which can provide real-time evaluation of patients. Compared with many other modalities, an ultrasound scan is easy to perform, substantially lower in cost, and it does not use harmful ionizing radiation. The research interest in robotizing ultrasound systems has always been a popular topic since the late 1990s within the European Union, North America, and Japan. This was because robotized ultrasound systems could potentially solve the deficiencies of the on-site manual manipulation of hand-held probes, such as difficulties of maintaining accurate probe positioning for long periods of time using human hands [1] and the requirements for experienced sonographers to be on-site [2]. Therefore, many proposed robots were mainly designed in the typical master-slave configuration, whereby the master-side sonographer can be in a remote location to perform the examination and a slave-side robot driving the ultrasound probe mimics the movements of the remote sonographer [3, 4]. These robotic ultrasound systems presented in the literature were mainly designed for diagnostic purposes but a few of them were also aimed at the assistance of needle insertions, interventional procedures, or open surgeries when ultrasound is used for guidance.

However, remote controlled ultrasound systems using robots with the master-slave configuration are still not adequate to solve the problem of general usability and reliable acquisition of ultrasound as they still require a manual control approach which is tedious, time consuming, and most of all experience-dependent. To facilitate autonomous and standardized ultrasound acquisition using machine intelligence, several works explore visual servoing techniques for tracking particular features, e.g., tracking the carotid artery using an extracorporeal ultrasound robot [5] and automatic scanning of the carotid artery using motion compensation [6]. Introduced by Wang et al., an automatic acquisition workflow for cardiac images using an intra-operative ultrasound robot has been studied in [7, 8]. The workflow includes the use of an ultrasound view planning platform, an auto-adaption algorithm of patient-specific data, and different probe tracking methods. Similarly, the workflow with pre-planning, patient-specific geometry adaption, and the according robotic control has also been studied by Esteban et al. for ultrasound-guided facet joint insertion [9].

Aiming at automated ultrasound examination in a uniform way, the iFIND (intelligent Fetal Imaging and Diagnosis) project is a recent ongoing research project that relates to the use of robotic systems to assist ultrasound examinations. The

Manuscript received: October 14, 2020; Revised: December 20, 2020; Accepted: January 12, 2021. This paper was recommended for publication by Editor Pietro Valdastri upon evaluation of the Associate Editor and Reviewers' comments. This work was funded by the Wellcome Trust IEH Award (102431) and supported by the Wellcome/EPSRC Centre for Medical Engineering (WT203148/Z/16/Z). *(James Housden and Shuangyi Wang are co-first authors.)*

Corresponding author: Shuangyi Wang (Shuangyi.wang@ia.ac.cn).

[1]J. Housden, X. Bao, E. Skelton, J. Matthew, O. Eltiraifi and K. Rhode are with the School of Biomedical Engineering and Imaging Sciences, King's College London, London SE1 7EH, UK.

[2]S. Wang is with the State Key Laboratory of Management and Control for Complex Systems, Institute of Automation, Chinese Academy of Sciences, Beijing 100190, China.

[3]J. Zheng is with the School of General Engineering, Beihang University, Beijing 100191, China.

[4]Y. Noh is with the Department of Mechanical and Aerospace Engineering, Brunel University, London UB8 3PH, UK.

[5]A. Singh and D. Singh are with the Xtronics, Ltd., Gravesend, Kent DA12 2AD, UK.

Digital Object Identifier (DOI): see top of this page.

project aims to improve the accuracy of routine 18-20 week screening in pregnancy by developing new computer-guided ultrasound technologies using multiple probes that will allow screening of fetal abnormalities with the assistance of robotics and AI. This was motivated by evidence that the diagnostic accuracy and sensitivity of ultrasound can be limited by technical restraints in the imaging. There is also strong evidence of major regional and hospital-specific variation in prenatal detection rates of major anomalies [10, 11].

With the rapidly growing field of image processing and machine learning techniques, several innovative deep learning-based ultrasound processing methods for fetal imaging have been proposed by the project, e.g., view detection [12] and shadow detection [13]. Moreover, our previous works have demonstrated the transformative value of using multiple probes or images to achieve extended field of view and improved quality, e.g., complete fetal head compounding [14] and quantification of placenta [15]. Working towards intelligence and autonomy, the combined use of these image processing techniques with robotic technology [16] would be a critical step as only a robotized tool can hold multiple probes accurately, facilitate standardization, and operate those computer-based algorithms in an executable way. Therefore, the aim of our robotic development has been set with the following requirements: (1) to be able to hold and manipulate multiple probes to reach target locations in flexible and safe manners; (2) to be able to operate the robot in a standardized way in acquisition to allow future integration with proposed ultrasound processing methods.

To provide a robotic tool to demonstrate the potential integrations, a dual-arm robot was decided to be the initial research object and this paper reports the design of the robot to meet the manipulation requirements and the motional planning approach to facilitate standardization. Compared with most of the other previous works on robotic ultrasound, the proposed system is the first dual-probe diagnostic robot, and it was designed to operate in a standardized way to integrate the newly developed ultrasound processing methods.

II. Design and Implementation of the Robot

A. Mechanical Design

An overview of the proposed robotic system is shown in Fig. 1. The final design of the dual-probe ultrasound robot has 17 degrees-of-freedom (DOFs) with two arms holding and controlling two ultrasound probes.

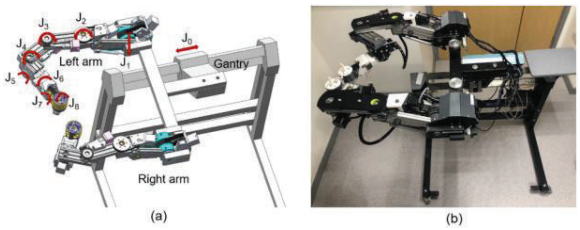

Fig. 1. Illustration of the iFIND dual-probe ultrasound robot: (a) schematic representation with joint definition and (b) the implementation of the system.

A side-mounted gantry system over the patient supported by a trolley system, with the two arms attached to the gantry coming in from the feet end, was configured as the working pose of the robot. The system includes one translational DOF for the gantry (J_0) driven by a linear belt mechanism, three rotational DOFs (J_1, J_2, and J_3) for each of the arms driven by worm gear and gear train mechanisms, and five rotational DOFs (J_4, J_5, J_6, J_7, and J_8) for each of the end wrist units driven by worm gear and gear train mechanisms. The redundant DOFs in the system were designed to allow the two ultrasound probes to be positioned and orientated flexibly while at the same time not colliding with each other. The total weight of the end wrist unit, which is normally positioned in close contact with patients, is less than 2 kg and the length of the unit is about 25 cm.

B. Safety features

1) Spring-ball based mechanical clutch: The mechanical safety of the proposed robot was emphasized with clutch mechanisms incorporated into J_1 – J_5, to limit the allowable force applied to the patient, the nearby health professionals and adjacent equipment when the robot is in action. An example clutch configuration (for J_2) is shown in Fig. 2(a). In the design, ball-spring pairs are inserted into the clutch detent holes. When the clutch is engaged, the inner clutch and the outer clutch are tightly locked, pushed by the preloaded spring. The inner and outer clutch would rotate simultaneously. When excessive torque is exerted on the joint, the clutch mechanism is triggered, which stops the torque transmission from the outer to the inner clutch with the balls pushed out from the detent holes. If the torque on the inner clutch decreases, the balls would re-engage and move into the next detent holes, locking the clutch again. Otherwise, the ball-spring pairs would keep rotating with the inner clutch and no torque is transmitted. Therefore, the torque is strictly limited to a safe threshold mechanically. Clutches that prevent excessive vertical force were designed based on our previous study [17], and clutches for the horizontally actuated joints were designed based on practical trials to ensure they are limited to generate tolerable force/torque when colliding with operators or equipment.

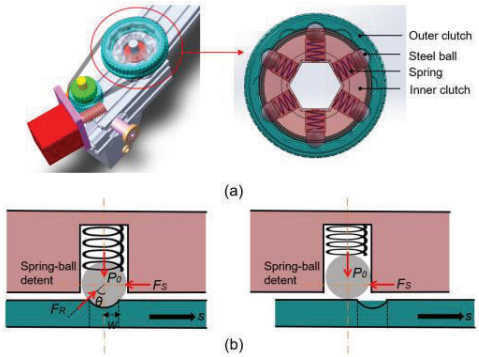

Fig. 2. Illustration of the spring-ball based mechanical clutch: (a) design of the clutch joint and (b) the explanation of the disengage mechanism.

When the clutch is not triggered, the detent structure is in its engaged position with the ball held by a preloaded spring compressed by the clutch cover (Fig. 2(b)). The preload is denoted as P_0 and the radius of the ball is denoted as R. The detent case contains the vertical compression spring with a spring constant k. When excessive force occurs, the detent slider slides horizontally over the detent case until the ball completely comes out from the detent hole. These two parts

develop a horizontal shear force F_s between them. Inside of the slider is the conical notch with its radius denoted as w, which generates the reaction force F_R in the angle of θ. During the triggering process, the horizontal force can be calculated based on the analysis in [17]. This is decided by the radius of the steel ball, conical notch radius, spring constant and the preload resulted from the initial compression. The triggering torques of $J_1 - J_5$ and the clutch parameters are summarized in Table I.

TABLE I
CHARACTERISTICS OF THE PROPOSED CLUTCHES

Parameters	J_3 & J_4	J_1 & J_2 & J_5
Radius of steel ball (s)	4 mm	4 mm
Conical notch radius (w)	3.62mm	3.815mm
Free length of spring (l_0)	15 mm	15 mm
Spring constant (k)	2 N/mm	2 N/mm
Spring outer diameter (d_0)	8 mm	8 mm
Compressed length of spring (Δl)	4.97mm	5.11 mm
Sliding force (F_s)	129.12N	194.58N
Preloaded force (P_0)	9.94N	10.22 N
Triggering torque (T)	2866.46N*mm	5442.40N*mm

2) Customized multi-axis force/torque sensor: customized six-axis force/torque sensor was designed. The proposed sensor can be clamped to hold the ultrasound probe. The sensor consists of two pieces which can form an 8-legged Stewart platform, as shown in Fig. 3. Each leg works as a cantilever beam to allow for a measurable displacement under an external load. The displacements of the legs were measured with eight light intensity-based optoelectronic sensors. The sensor was calibrated and compared to the ATI Mini40 sensor by measuring sequences of forces and torques, and the maximum errors of force/torque components (F_x, F_y, F_z, M_x, M_y, M_z) were found to be 16.3%, 20.0%, 27.5%, 20.5%, 21.6%, and 14.9% when compared with a commercial force/torque sensor. Details of the design, analysis and discussion of the sensor can be found in our previous publication [18]. The proposed sensor is intended to be used together with a force control scheme to measure and regulate the contact force between the ultrasound probe and the abdominal tissues. It has been demonstrated that the robot is able to slide across the surface while maintaining contact with and normal alignment to the surface at a desired target axial force, as illustrated in our previous work [19].

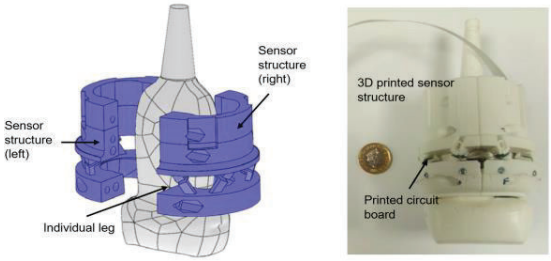

Fig. 3. Diagram of the customized multi-axis force/torque sensor.

3) Additional safety features: the electrical system of the robot has been carefully designed by including noise-reduction components, power dissipation components, a safety relay, and a user-controllable emergency button. The robot will stop moving immediately if the emergency button is pressed. Both the patient and the operator have access and the operator should reset the robot after the concern is addressed. In terms of software, safety control has been implemented with the capability to predict and indicate potential collisions of the two probes during the movements of the robot. This will provide the user with a warning signal in the display panel of the software. Moreover, a specially designed initial calibration sequence using homing sensors in each joint was implemented to allow the robot to be automatically initialized and recovered from failure modes.

C. Software and Control Inputs

The basic control of the robot can be done by operating the custom-written software (Fig. 4(a)), which includes the function to load an abdominal surface, read force sensing values, control each joint's movement and probe's movement based on the kinematics. A customized control panel (Fig. 4(b)) was made to work as an alternative control input to work together with the control software. The panel includes large buttons to select the activated arm, a set of small buttons (yellow, blue, and green) to translate the probe, another set of buttons (white) to axially rotate the probe, a joystick to rotate the probe in lateral and elevational directions, and a set of LEDs to indicate the level of the sensed contact force in the vertical direction.

Fig. 4. (a) The robot control software and (b) the customized control panel.

III. STANDARDIZED ACQUISITION WORKFLOW

A. Overview

Using the proposed dual-probe robot, we have proposed the following standardized robotic-assisted acquisition workflow (Fig. 5) to deal with different shapes of the patient's belly and operate the robot in a consistent way to go to a desired location.

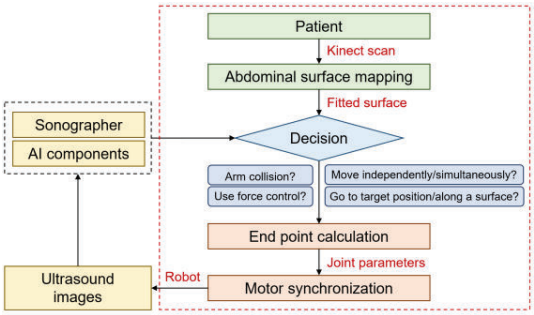

Fig. 5. Diagram of the standardized robotic-assisted acquisition workflow.

The motion planning strategy, as introduced in section III.B, summarizes the overall position control to move the two probes independently or as a single unit along the patient body without collisions of the arms and maintaining a safe offset of the robot from the patient's abdomen. This can be combined with standard force control to regulate the vertical distance of the

probe and improve probe contact and alignment to the surface at a desired target axial force, as introduced in our previous work [19]. The abdominal surface mapping, as introduced in section III.C, deals with adaption to the geometric information of the patient's belly. The end point calculation and joint synchronization are the detailed mathematical approach serving as the rule-based inverse kinematics and motor control method, as introduced in sections III.D and E.

B. Motion Planning

Since the robot has 17 degrees of freedom (DOFs), it is a complex task to control the position of the two ultrasound probes around the abdomen simultaneously. Sometimes the probes need to move independently, for example keeping one stationary while moving the other to a new position, but it is sometimes also useful to move the two as a single unit. For example, to maintain an extended field of view while sweeping along the length of a fetus, the probes need to keep the two images in the same plane as each other. This all needs to be achieved while avoiding collisions of the arms and maintaining a safe offset of the robot from the patient's abdomen.

With 17 DOFs to position the two probes, there is more than one way to reach each position. The aim here is to use a closed-form solution for any target position. By doing this, we can ensure that there will always be a solution that, by design, avoids collisions of the two robot arms and maintains a safe clearance from the abdomen.

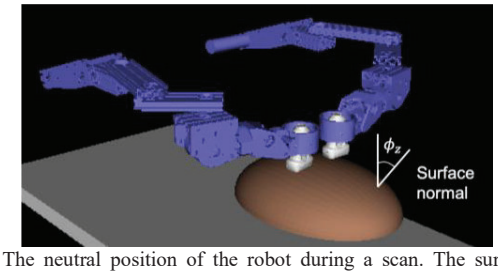

Fig. 6. The neutral position of the robot during a scan. The surface of a pregnant abdomen is modelled here as an ellipsoid. The angle ϕ_z is the direction of the surface normal from the vertical at a point on the surface.

The approach taken here is to consider the problem in two parts: (1) appropriate joint positions are calculated to achieve the end point of the movement (the target) and (2) each motor is moved to achieve a smooth motion towards this end point. The required workspace of the robot assumes an approximately ellipsoidal abdomen, where the probes may need to be placed normal to the surface anywhere on the upper half of the ellipsoid, and they may also need to tilt through a range of angles in these positions. Fig. 6 shows the robot in its neutral position over a model ellipsoidal surface of a typical size for a pregnant abdomen. In actual scanning, the shape of the abdominal surface can vary widely between patients and is therefore measured as part of the scanning protocol to assist with the motion planning calculations.

C. Abdominal Surface Mapping

The shape of a patient's abdomen is measured prior to the scan using a Kinect camera. The camera data is processed using the Kinect Fusion software available in the Kinect for Windows Developer Toolkit. This software automatically creates a surface mesh representing the abdominal surface. The surface mesh is often noisy and incomplete, and it needs to be further processed to fill holes and ensure a smooth surface model. This is achieved by fitting a non-parametric spline surface to the recorded point data with a grid of 13×13 control points. An example fitted surface is shown in Fig. 7.

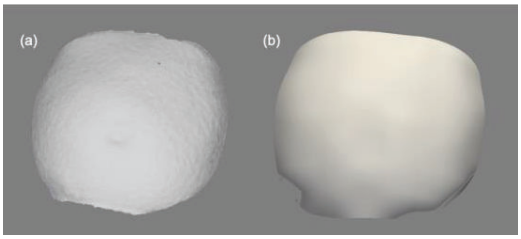

Fig. 7. (a) The surface of a pregnant abdomen measured with the Kinect camera, shown after cropping surrounding structures. (b) A non-parametric spline surface fitted to the mesh data.

D. End Point Calculation

The 17 DOFs of the robot would usually allow extra flexibility and multiple different ways to reach a target; here this flexibility is constrained to ensure that the robot will be in a known position for any target. This is done by using each joint for a specific purpose in reaching a pose, and by calculating the joint angles in a pre-defined order.

First, joints J_4 and J_5 on each arm are angled so that the end wrist unit (the part of the arm from J_4 to the ultrasound probe), are positioned over the abdomen according to the angle of the abdominal surface. In most cases, this positions the end wrist tangentially to the surface. Second, with the location and orientation of the wrist defined, the angles of J_6 to J_8 are calculated to orient the probe to the target angle on the surface. These joints are on three orthogonal axes and can achieve any orientation that may be needed by the probe. Third, the position of J_1 on each arm is calculated to set the correct vertical position of each probe. Fourth, the linear translation of the gantry is adjusted so that both arms are working near the center of their range in the head-feet direction. Finally, the positions of the remaining joints J_2 and J_3 on each arm, which together form a horizontal 2-bar mechanism, are calculated to set the correct horizontal for each probe.

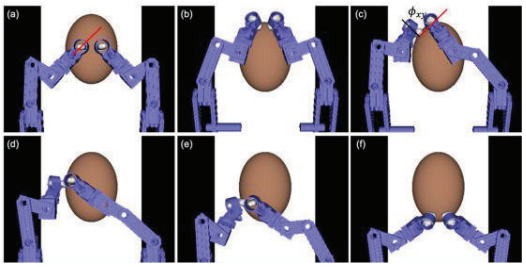

Fig. 8. Examples of the positions taken by the robot to reach different parts of the abdomen. The red vectors in (a) and (c) show the neutral direction of the right arm. The angle ϕ_{xy} is the angle from the neutral direction to the surface normal.

The most complex part of this calculation is the first step of setting orientations for the wrists (J_4 and J_5). Given a target pose for one of the probes, the angle of the wrist depends on the orientation of the surface below it, as defined by the surface normal at the point closest to the probe face in the target pose.

Each wrist also has a neutral orientation which is defined according to the direction the arm approaches the abdomen (shown in Fig. 8a). The normal and the neutral direction define two angles: ϕ_z shown in Fig. 6 and ϕ_{xy} shown in Fig. 8c. The angle of joint J_4 downwards from the horizontal is set according to $J_4 = 90° \times \left(\frac{\phi_z}{90°}\right)^{\alpha}$, where α is an adjustable parameter set to 2. The joint J_5 angle varies with ϕ_z and ϕ_{xy} from the neutral direction as follows:

$$J_5 = (1 - w_z) \times \begin{cases} \left|180° - |\phi_{xy}|\right| \times -45°, & -180° < \phi_{xy} < -135° \\ -45°, & -135° \le \phi_{xy} < -45° \\ \phi_{xy}, & -45° \le \phi_{xy} \le +45° \\ +45°, & +45° < \phi_{xy} \le +135° \\ \left|180° - |\phi_{xy}|\right| \times +45°, & +135° < \phi_{xy} \le +180° \end{cases}$$

where $w_z = \cos^{\beta}(\phi_z)$ and β is an adjustable parameter set to 5. For a probe placed on the top center of the abdomen, the wrist would be in its neutral orientation, as in Fig. 8a. As it moves away from the center towards the steeper sides of the abdomen, as indicated by the angle ϕ_z, the wrist orientation is adjusted to follow the surface angle (Fig. 8b-f). On the side of the abdomen from which the arm approaches (towards the patient's feet), the wrist is not able to orient to the surface but instead angles down towards the surface (Fig. 8e). These wrist positions are designed to allow smooth transitions from one position to another, which allows sweeping of the probe along any line of the abdomen.

E. Joint Synchronization

Once the joint angles to reach a target position have been calculated, the movement is started. The motors in the robot are stepper motors that are controlled through a trapezoidal velocity sequence of acceleration to maximum speed and deceleration to complete a movement. To synchronize the joints and acquire a smooth motion, the time that each motor would take to run to its target position is calculated, assuming its usual maximum speed. This calculation allows the motor to be already running at a non-zero speed at the start of the movement. With these times calculated, the longest running time among the 17 motors is noted. Finally, for all the other motors, a reduced maximum speed is calculated so that they take the same time to reach the target as the slowest motor. In this way, all motors finish their movement at the same time. Other than this requirement for the motors to reach their target simultaneously, there is no restriction on the path taken by the probe. Therefore, movements are made in small steps to avoid the probes trying to pass through the abdomen.

IV. Preliminary Assessments

A. Simulation Experiments

The end-point calculation was evaluated by testing the range of reachable positions on the ellipsoidal surface (obtained based on a fetal ultrasound phantom with realistic belly shape), and the proximity of different parts of the robot to the abdomen in each position. Target probe positions were tested over a grid on the surface of the abdomen of 40x40 cm, in steps of 2 cm. The probes were moved to each location as a synchronized pair. Three different axial orientations of the probe pair were tested with the probes aligned side-by-side to view an extended plane, as shown in Fig. 9. At each location, it was first noted whether the robot could reach that position within the range of its mechanism and joints, and then the shortest distance from each link of the robot to the abdominal surface was calculated.

Fig. 9 shows the results of the range and proximity test for the three angles of the probe pair. The grey regions of the abdomen show where the robot was unable to reach the target position. The coloured regions are where the robot was able to reach the target. This was possible at 172 of the target points in the lateral probe configuration, 129 in the 45° configuration, and 108 in the sagittal configuration. The two probes were separated on the surface by 100 mm and the location of the colour is the mid-point of the two probe locations. Therefore, the robot's maximum range with at least one probe is 50 mm beyond the coloured region. The colourmap shows the proximity of the robot in these regions. The important links to consider are those of the wrist (those actuated by joints J_4 to J_8 on each arm); the back ends of the arms are always far above the abdomen. In the configurations tested, the ultrasound probes are always in contact with the abdomen, and the links holding the probes as well as the end rotation links were found to be consistently close to the abdomen with a minimum distance in any position of 48 mm. The result shown in Fig. 9 is for the arm on the right side of the abdomen (left side of the figures). The results for the other arm are symmetrical to this.

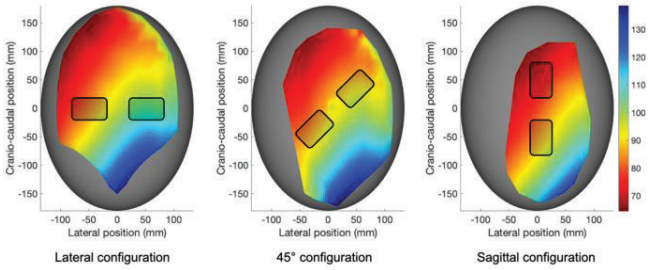

Fig. 9. Range and proximity results with the probes arranged side-by-side to acquire an extended image plane in one of the three directions shown. The plots represent the abdomen viewed from above with the patient's head towards the top of the page. The colours show the shortest distance to the abdomen in mm from the robot link actuated by joint J_5 in the right arm. The closest proximity measured for this link in any configuration is 64.5 mm. The rectangular outlines show the position of the probe pair in each configuration.

B. Volunteer study

To provide evidence for in-vivo tests, we applied for and obtained ethical approval to test our robots on non-pregnant healthy volunteers for general abdominal scans before the system is clinically approved to be used on pregnant participants. The volunteer study (Approved by the King's College London local ethics committee, study title: Investigating Robotic Abdominal Ultrasound Imaging, Study reference: HR-17/18-5412) using the proposed dual-probe robot is shown in Fig. 10.

For the setup, the robotic system was located at the left side of the bed controlled and monitored by the engineer while the sonographer controls the ultrasound machine on the right side of the bed. Following the standardized acquisition workflow

introduced in Section III, we utilized a Kinect scanner to acquire the abdominal surface of the volunteer and imported that into the robot software. Based on the kinematics, the motion planning and surface following abilities of the robots were tested in which case the target positions of the probe were provided by the Kinect scan and the robots would control the probe to follow the abdominal surface and reach target positions. The current initial alignment was done by manually position the robot at the middle of the belly using the umbilicus as a reference after loading the scanned surface. A marker points-based registration method using Kinect could be further developed to achieve more accurate alignment. During the manipulation, the sonographer would manipulate the robot, i.e., probe pose, via the control panel to acquire standard views for general abdominal scan targeting at the anatomical structures.

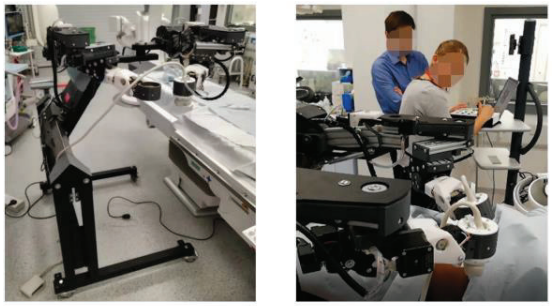

Fig. 10. Experimental setup for the volunteer tests: (a) perspective view of the robot and (b) the user interaction with the robot via the control panel.

Based on the described experimental protocol using the proposed robot, four volunteer tests were performed and the technical functionalities of the robot have been successfully verified. We further analysed the images obtainable, compared to the sonographer scanning manually. In each volunteer, the sonographer aimed to exam the pancreas, kidney, liver, and aorta manually and robotically by capturing standard views, e.g., pancreas, aorta (AO), gallbladder (GB), right kidney (RK), right lobe of liver (RLL), and left lobe of liver (LLL).

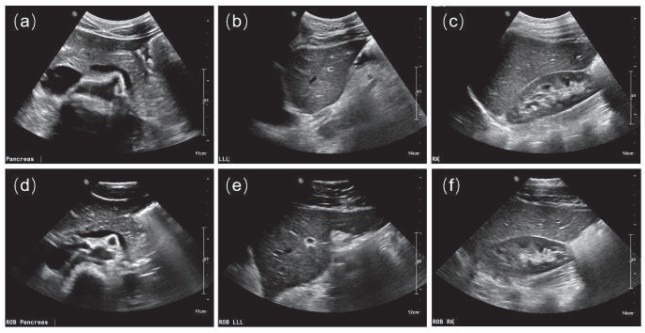

Fig. 11. Ultrasound images acquired by sonographer (a-c) and robot (d-f) for pancreas (a, d), LLL (b, e) and RK (c, f) views.

For those of the views that are both successfully captured manually and robotically, the images were then scored by a sonographer for image quality as ‘good’, ‘acceptable’ and ‘poor’ according to the image quality component of the British Medical Ultrasound Society Peer Review Audit Tool 2014 v3 [20]. In total, 40 views were selected for comparison, 20 by sonographer and 20 by robot. The proportion of images with ‘good’ or ‘acceptable’ quality was 100% for sonographer and 95% for the robot. Of the images with ‘good’ or ‘acceptable’ quality scores, the sonographer achieved a ‘good’ image in 60% of images, while the robot achieved this in 40% of images. Example views acquired manually and robotically are shown in Fig. 11. In both cases, the regions of interest are well positioned in the image. The contrast in the robot-acquired images is similar to the one in the manually obtained images.

V. Discussion and Conclusion

In this paper, we have presented a robotic system for fetal ultrasound scanning with specially designed safety features and a standardized acquisition workflow. The robot has included several customized safety features, e.g., the mechanical-based safety clutch and the active multi-axis force/torque sensor. Detailed studies and verifications of these specific safety features can refer to our previous publications [17, 18]. Specifically, a potential concern using the proposed safety clutch is that the joint would have the wrong rotation information when it is triggered. In this scenario, the corresponding joint would attempt to move but constrained by the clutch, resulting in small amounts of movements back and forth. This can be observed by the sonographer and one should then re-engage the clutch manually, investigate the cause, and reset the corresponding joint to the home position. For a commercial-ready product that we are now working towards, the stepper motors will be replaced by servo motors with individual position tracking capability to resolve this concern.

By performing simulation experiments, we also evaluated the robot’s ability to safely reach all regions of the abdomen. The results show that it is able to reach a good range of positions on the abdomen, but it is limited on the caudal side as the abdomen begins to slope down. This is caused by the abdomen sloping down on the near side to the robot arm, which requires the wrist to tilt down almost perpendicular to the abdomen and sometimes requires the end rotation joints to be outside their range. This suggests that some further improvements of the robot or increase in joint range will be necessary to adequately perform a fetal scan. It is also notable that in the 90° rotated configuration of the probes used to image sagittal planes, the robot is unable to reach as far to the sides of the abdomen as in the lateral configuration. This is because in the lateral configuration of the two probes, the left probe is nearer the left side of the abdomen, so that the left arm does not need to reach as far across the abdomen, and therefore the pair of probes can reach further.

The significance of the proximity measurements is the requirement for the robot to move safely around the abdomen. In this unrealistic situation of a rigid abdomen in a perfect ellipsoidal shape, we can guarantee that the robot will always be at least 48 mm from the surface. However, on a real abdomen, the probe may indent the surface by several cm. In the more extreme indentations, the end links of the robot may come into contact with the patient, and it will be essential to ensure that they do this in a safe way. It is much less likely that the less distal links of the robot would ever touch the abdomen. Moreover, a limitation of the motion planning is that it only calculates the inverse kinematics for the target pose. While we can be sure that the robot will reach the correct end pose safely

the method puts no constraints on how the probe moves towards the target. There is certainly no guarantee that it will move in a straight line. Over short distances, this does not have a noticeable effect, and if straight line or surface following motion is desired then one solution would be to divide the movement into a sequence of smaller steps.

With the successful completions of four volunteer tests using the standardized acquisition workflow in a clinical environment, the robustness of the robot in terms of its mechanical, electrical and control systems have been preliminarily verified. We have shown that our robot is capable of safely reaching a range of positions around the abdomen and acquire required ultrasound images in a more standardized way. However, more thorough analyses and clinical studies are required to guarantee this for more realistic ranges of abdominal shapes, and some improvements of the robot or kinematics algorithms may be needed. Moreover, follow-up experiments to integrate the other proposed image processing methods within the project, e.g. view detection and field-of-view extension [12, 14] would demonstrate the intelligent use of the system, with more quantitative results to assess the quality of the acquired ultrasound views and the levels of autonomy.

To conclude, it is encouranging that the robot can be used in the future to achieve our goal of standardized scanning with the combination of the current proposed workflow and AI-based image analysis algorithms. The future prospect would be transforming how fetal screening is currently performed and be able to assist less qualified operators to obtain accurate diagnostic results.

REFERENCES

[1] N. Magnavita, L. Bevilacqua, P. Mirk, A. Fileni and N. Castellino, "Work-Related Musculoskeletal Complaints in Sonologists," *J. Occup. Environ. Med.*, vol. 41, no. 11, pp. 981–988, 1999.

[2] L. LaGrone, V. Sadasivam, A. Kushner and R. Groen, "A review of training opportunities for ultrasonography in low and middle income countries," *Tropical Med. Int. Health*, vol. 17, no. 7, pp. 808–819, 2012.

[3] A. Priester, S. Natarajan, and M. Culjat, "Robotic ultrasound systems in medicine," *IEEE Trans. Ultrason. Ferroelectr. Freq. Control*, vol. 60, no. 3, pp. 507–523, 2013.

[4] D. R. Swerdlow, K. Cleary, E. Wilson, B. Azizi-Koutenaei, and R. Monfaredi, "Robotic Arm–Assisted Sonography: Review of Technical Developments and Potential Clinical Applications," *AJR. Am. J. Roentgenol*, vol. 208, no. 4, pp. 733–738, 2017.

[5] P. Abolmaesumi, S. Salcudean, W.-H. Zhu, M. Sirouspour, and S. Dimaio, "Image-guided control of a robot for medical ultrasound," *IEEE Trans. Robot.*, vol. 18, no. 1, pp. 11–23, 2002.

[6] R. Nakadate, J. Solis, A. Takanishi, M. Sugawara, K. Niki, and E. Minagawa, "Development of the Ultrasound Probe Holding Robot WTA-1RII and an Automated Scanning Algorithm based on Ultrasound Image Feedback," in *ROMANSY 18 Robot Design, Dynamics and Control*, Vienna, Austria, 2010, pp. 359–366.

[7] S. Wang, J. Housden, D. Singh, K. Althoefer, and K. Rhode, "Design, testing and modelling of a novel robotic system for trans-oesophageal ultrasound," *Int. J. Medical Robot. Comput. Assist. Surg.*, vol. 12, no. 3, pp. 342–354, 2016.

[8] S. Wang, D. Singh, D. Johnson, K. Althoefer, K. Rhode and R. J. Housden, "Robotic Ultrasound: View Planning, Tracking, and Automatic Acquisition of Transesophageal Echocardiography," *IEEE Robot. Autom. Mag.*, vol. 23, no. 4, pp. 118–127, 2016.

[9] J. Esteban, W. Simson, S. R. Witzig, A. Rienmüller, S. Virga, B. Frisch, O. Zettinig, D. Sakara, Y.-M. Ryang, N. Navab, and C. Hennersperger, "Robotic ultrasound-guided facet joint insertion," *Int. J. Comput. Assist. Radiol. Surg.*, vol. 13, no. 6, pp. 895–904, 2018.

[10] H. Kilner, M. Wong, and M. Walayat, "The antenatal detection rate of major congenital heart disease in Scotland," *Scott. Med. J.*, vol. 56, no. 3, pp. 122–124, 2011.

[11] "Variation in Prenatal Diagnosis of Congenital Heart Disease in Infants," *Pediatrics*, vol. 136, no. 2, 2015.

[12] C. F. Baumgartner, K. Kamnitsas, J. Matthew, T. P. Fletcher, S. Smith, L. M. Koch, B. Kainz, and D. Rueckert, "SonoNet: Real-Time Detection and Localisation of Fetal Standard Scan Planes in Freehand Ultrasound," *IEEE Trans. Med. Imaging*, vol. 36, no. 11, pp. 2204–2215, 2017.

[13] Q. Meng, J. Housden, J. Matthew, D. Rueckert, J. A. Schnabel, B. Kainz, M. Sinclair, V. Zimmer, B. Hou, M. Rajchl, N. Toussaint, O. Oktay, J. Schlemper, and A. Gomez, "Weakly Supervised Estimation of Shadow Confidence Maps in Fetal Ultrasound Imaging," *IEEE Trans. Med. Imaging*, vol. 38, no. 12, pp. 2755–2767, 2019.

[14] R. Wright, *et al*., "Complete Fetal Head Compounding from Multi-view 3D Ultrasound," in *Proc. Int. Conf. Medical Image Computing and Computer Assisted Intervention*, in Lecture Notes in Computer Science, vol. 11766, 2019, pp. 384–392.

[15] V. Zimmer, *et al*., "Towards Whole Placenta Segmentation at Late Gestation Using Multi-view Ultrasound Images," in *Proc. Int. Conf. Medical Image Computing and Computer Assisted Intervention*, in Lecture Notes in Computer Science, vol. 11768, 2019, pp. 628–636.

[16] S. Wang, J. Housden, Y. Noh, D. Singh, A. Singh, E. Skelton, J. Matthew, C. Tan, J. Back, L. Lindenroth, A. Gomez, N. Toussaint, V. Zimmer, C. Knight, T. Fletcher, D. Lloyd, J. Simpson, D. Pasupathy, H. Liu, K. Althoefer, J. Hajnal, R. Razavi, and K. Rhode, "Robotic-Assisted Ultrasound for Fetal Imaging: Evolution from Single-Arm to Dual-Arm System," in *Proc. Annu. Conf. Towards Autonomous Robotic Systems*, in Lecture Notes in Computer Science, vol. 11650, 2019, pp. 27–38.

[17] S. Wang, *et al*., "Analysis of a Customized Clutch Joint Designed for the Safety Management of an Ultrasound Robot," *Appl. Sci.*, vol. 9, no. 9, p. 1900, 2019.

[18] N. Yohan, *et al.* "A 2-piece six-axis force/torque sensor capable of measuring loads applied to tools of complex shapes," in *Proc. 2019 IEEE/RSJ Int. Conf. Intelligent Robots and Systems*, Macau, China, pp. 7976–7981.

[19] J. Housden, et al. " Control Strategy for a New Extra-corporeal Robotic Ultrasound System," presented at the MEIBioeng/MPEC Conference 2017, London, UK, Sept. 13–14, 2017.

[20] "British Medical Ultrasound Society Peer Review Audit Tool 2014 v3", Bmus.org, 2020. [Online]. Available: https://www.bmus.org/static/uploads/resources/Peer_Review_Audit_Tool_wFYQwtA.pdf. [Accessed: 22- Aug- 2020].